Available online at www.sciencedirect.com
SCIENCE DIRECT®
Geochimica et Cosmochimica Acta 70 (2006) 2127–2139
Geochimica
www.elsevier.com/locate/gca

Petrography and geochemistry of the chassignite Northwest Africa 2737 (NWA 2737)

P. Beck [a,*], J.A. Barrat [b], Ph. Gillet [a], M. Wadhwa [c], I.A. Franchi [d], R.C. Greenwood [d], M. Bohn [b], J. Cotten [b], B. van de Moortèle [a], B. Reynard [a]

[a] *Laboratoire des Sciences de la Terre, CNRS UMR 5570, Ecole Normale Supérieure de Lyon, 46 allée d'Italie, 69364 Lyon Cedex 7, France*
[b] *U.B.O.-I.U.E.M., CNRS UMR 6538 (Domaines Océaniques), place Nicolas Copernic, F-29280 Plouzané Cedex, France*
[c] *Department of Geology, The Field Museum, 1400 S. Lake Shore Dr. Chicago, IL 60605, USA*
[d] *Planetary and Space Science Research Institute, The Open University, Walton Hall, Milton Keynes, MK7 6AA, UK*

Received 12 October 2005; accepted in revised form 17 January 2006

Abstract

We report on the petrology and geochemistry of the Northwest Africa 2737 (NWA 2737) meteorite that was recovered from the Morrocan Sahara in 2000. It is the second member of the chassignite subclass of the SNC (Shergotitte-Nakhlite-Chassignite) group of meteorites that are thought to have originated on Mars. It consists of black olivine- and spinel-cumulate crystals (89.7 and 4.6 wt%, respectively), with intercumulus pyroxenes (augite 3.1 wt% and pigeonite–orthopyroxene 1.0 wt%), analbite glass (1.6 wt%) and apatite (0.2 wt%). Unlike Chassigny, plagioclase has not been observed in NWA 2737. Olivine crystals are rich in Mg, and highly equilibrated ($Fo = 78.7 \pm 0.5$ mol%). The black color of olivine grains may be related to the strong shock experienced by the meteorite as revealed by the deformation features observed on the macroscopic to the atomic scale. Chromite is zoned from core to rim from $Cr_{83.4}Uv_{3.6}Sp_{13.0}$ to $Cr_{72.0}Uv_{6.9}Sp_{21.1}$. Pyroxene compositional trends are similar to those described for Chassigny except that they are richer in Mg. Compositions range from $En_{78.5}Wo_{2.7}Fs_{18.8}$ to $En_{76.6}Wo_{3.2}Fs_{20.2}$ for the orthopyroxene, from $En_{73.5}Wo_{8.0}Fs_{18.5}$ to $En_{64.0}Wo_{22.1}Fs_{13.9}$for pigeonite, and from $En_{54.6}Wo_{32.8}Fs_{12.6}$ to $En_{46.7}Wo_{44.1}Fs_{9.2}$ for augite. Bulk rock oxygen isotope compositions confirm that NWA 2737 is a new member of the martian meteorite clan ($\Delta^{17}O = 0.305 \pm 0.02‰$, $n = 2$). REE abundances measured in NWA 2737 mineral phases are similar to those in Chassigny and suggest a genetic relationship between these two rocks. However, the parent melt of NWA 2737 was less evolved and had a lower Al abundance.

1. Introduction

The number of known martian meteorites has nearly doubled in the past decade, with more than thirty members being now recognized. All these rocks plot on a single O isotopic fractionation line and share petrological and chemical features, which indicate that they originate from the same large planetary body, most likely Mars. They range from basaltic rocks (the shergottites) to a variety of pyroxenitic (the nakhlite clinopyroxenites and the ALH 84001 orthopyroxenite) or dunitic (Chassigny) cumulates. Before the discovery of NWA 2737, Chassigny was the only dunitic sample among the known martian meteorites. In this article, we describe the petrology and geochemistry of a second chassignite (of total mass 611 g), which has been found in the Morrocan Sahara, and provide a comparison with Chassigny. During the reconnaissance study, this meteorite was nicknamed Diderot, after the French encyclopedist born in the city of Langres, a few kilometers from the village of Chassigny.

* Corresponding author. Present address: Geophysical Laboratory, Carnegie Institution of Washington, 5251 Broad Ranch Road NW, Washington, DC 20015, USA.
E-mail address: pbeck@ens-lyon.fr (P. Beck).

0016-7037/$ - see front matter © 2006 Elsevier Inc. All rights reserved.
doi:10.1016/j.gca.2006.01.016

2. Samples and analytical techniques

Petrographic observations and quantitative chemical analyses of the various mineralogical phases were made on two polished sections. Backscattered electron (BSE) images were obtained with a JEOL 840 scanning electron microscope at GEMPPM (Groupe d'Etude de Métallurgie Physique et de Physique des Matériaux). Major and minor chemical element abundances were measured using a CAMECA SX50 electron microprobe located in the research centre of IFREMER (Institut Français de Recherche pour l'Exploitation de la Mer) at Brest. Analyses were performed on WDS spectrometers at an accelerating voltage of 15 kV, a beam current of 12 nA and a 1 μm-sized beam spot. International mineral standards were used (orthose, albite, wollastonite, forstérite, chromite, hematite, ilmenite, aluminium oxide, corundum, and apatite). The detection limit for the analyzed elements is 0.005% oxide weight percent.

Sample for TEM observations was prepared by crushing in corundum crucible. Powder was deposited in holey carbon coated TEM copper grids in ethanol suspension and was dried. A JEOL 2010F instrument at CLYME (Consortium Lyonnais de Microscopie Electronique) in Lyon, operating at 200 kV, has been used for high resolution TEM imaging. This microscope is equipped for the chemical nano-analysis (probe size typically 2 nm for the investigation of nanometric features) with an EDX analyzer (Inca Oxford).

A 500 mg fragment was finely ground using a boron carbide mortar and pestle. Major and trace element concentrations were determined at the Université de Bretagne Occidentale in Brest, by ICP–AES (inductively coupled plasma–atomic emission spectrometry) and ICP–MS (inductively coupled plasma–mass spectrometry) using the procedure described by Cotten et al. (1995) and Barrat et al. (2000), respectively. The accuracy on major and trace element concentrations is better than 5%. The reproducibility is always better than 3% for the major elements and the Rare Earth elements (REE)) based on various standard and sample duplicates.

REE concentrations were determined in-situ in NWA 2737 phases with the Washington University modified Cameca IMS-3f ion microprobe. Experimental techniques for such measurements have been described in detail by Zinner and Crozaz (1986) and Lundberg et al. (1988). Typical primary (O^-) beam currents used in this study ranged from $\sim$<1 nA (for REE-rich phases like apatite) to $\sim$10 nA (for REE-poor minerals such as olivine), and corresponding beam spot sizes ranged from $\sim$10 to $\sim$50 μm. Errors (1σ) from counting statistics only are typically in the range of 5–10%.

Raman spectra were recorded with a Labram HR spectrometer equipped with confocal optics and a CCD detector at the Laboratoire des Sciences de la Terre, ENS Lyon. A microscope was used to focus the excitation laser beam (514 nm lines of a Spectra Physics® Ar + laser) to a 2 μm spot and to collect the Raman signal in the backscattered direction. Collecting times lasted between 10 and 60 s under small power (2–30 mW), to avoid sample deterioration.

Analytical details for the oxygen 3-isotope analyses are given in Miller et al. (1999). Briefly, 1–2 mg aliquots of powdered sample were heated with a CO_2 laser (10.6 nm) in the presence of BrF_5 to quantitatively liberate oxygen gas. Following purification the gas generated is analyzed on a PRISM III (VG Micromass, UK) to determine the $\delta^{17}O$ and $\delta^{18}O$ values. Analytical precision (2σ) is typically $\pm 0.08‰$ for $\delta^{18}O$ and $\pm 0.024‰$ for $\Delta^{17}O$.

3. NWA 2737: a new SNC meteorite

The classification of NWA 2737 in the SNC (martian) meteorite group was first suggested from the striking petrographical similarities with Chassigny and then confirmed by chemical measurements. Various elemental ratios have been used in order to discriminate between the different types of basaltic achondrites (e.g., Treiman et al., 2000). Key element ratios such as $(Fe/Mn)_{olivine}$ ($\approx$55), $(Na/Al)_{Bulk}$ ($\approx$0.35), and Ga/Al (3.1×10^{-4}) indicate that NWA 2737 is a new member of the martian meteorite clan.

This conclusion is confirmed by the oxygen isotope composition of NWA 2737. The two bulk rock measurements yield $\delta^{17}O = 2.40‰$, $\delta^{18}O‰ = 4.02‰$ ($\Delta^{17}O = 0.315‰$) and $\delta^{17}O = 2.30‰$, $\delta^{18}O‰ = 3.85‰$ ($\Delta^{17}O = 0.295‰$). These values lie on the mass fractionation line defined by the other martian meteorites (Clayton and Mayeda, 1996; Franchi et al., 1999), and are similar to the oxygen isotopic composition of Chassigny ($\delta^{17}O = 2.49‰$, $\delta^{18}O‰ = 4.20‰$, and $\Delta^{17}O = 0.306‰$); (Franchi et al., 1999).

4. General description

Unlike Chassigny, which has a pale green color, NWA 2737 is a crumbly dark rock (Fig. 1). It has a cumulate texture very similar to Chassigny, dominated by millimeter-sized anhedral to subhedral olivine crystals, with rare poikilitic augite (Fig. 2A). The modal mineralogy is that of a dunite (calculated from bulk analysis and mineral chemistry, in wt%): olivine 89.6%, augite 3.1%, spinel 4.6%, analbite 1.6%, orthopyroxene-pigeonite 1.0%, and phosphate 0.2%. The only noticeable difference with the mode of Chassigny is the absence of plagioclase (Floran et al., 1978). Based on textural observations, the following crystallization sequence can be inferred: spinel, spinel + olivine, intercumulus phases (K-feldspar, pyroxenes, apatite, sulfide; Fig. 3). Olivine and spinel contain magmatic inclusions up to 150 μm in diameter (Fig. 4), made of pyroxenes, olivine, (K, Si, Al)-rich glass, apatite, and possibly also kaersutitic amphibole. Carbonates are often encountered around the silicate crystals or in small veins within olivine grains.

Like Chassigny, NWA 2737 exhibits shock features probably related to its ejection from Mars. Olivines are

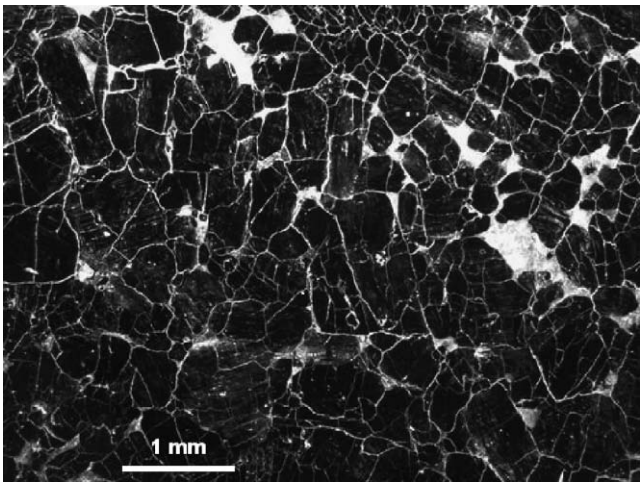

Fig. 1. An image of a thick section of NWA 2737 obtained under a binocular microscope with radial illumination with white light. The stone is dominated by dark olivine, together with euhedral chromite (dark), pyroxene, maskelynite, and glass (both clear and transparent). The white irregular fractures are typically filled with carbonates (calcite or aragonite).

mostly black in transmitted light, and are responsible for the overall dark aspect of the meteorite (Fig. 1). These black olivines are crosscut by a high density of planar shock defects. Feldspar has been transformed into maskelynite glass. This shock metamorphism has not perturbed the original magmatic texture of the meteorite.

5. Mineralogy and mineral chemistry

Representative electron microprobe analyses of mineral phases are presented in Table 1. Olivine crystals show a narrow chemical range ($Fo_{78.2–79.1}$), suggesting a high degree of post-magmatic equilibration. There is no evidence of chemical zoning in NWA 2737 olivines. They have a mean forsterite content of $Fo = 78.7$ mol%, significantly higher than olivines from Chassigny ($Fo = 69$ mol%). Their CaO, NiO, and MnO contents are lower than in Chassigny olivines.

Three pyroxenes are present: high-Ca pyroxene (augite), pigeonite, and orthopyroxene as demonstrated by the chemical analyses and Raman spectra (Table 1 and Fig. 5). Low-Ca pyroxenes occur as interstitial post-cumulus phases, in some case exhibiting thin (1 μm width) exsolved augite lamellae (Fig. 2C). The three types of pyroxenes are not chemically homogeneous. Compositions range from $En_{78.5}Wo_{2.7}Fs_{18.8}$ to $En_{76.6}Wo_{3.2}Fs_{20.2}$ for the orthopyroxene, from $En_{73.5}Wo_{8.0}Fs_{18.5}$ to $En_{64.0-Wo_{22.1}Fs_{13.9}}$ for pigeonite, and from $En_{54.6}Wo_{32.8}Fs_{12.6}$ to $En_{46.7}Wo_{44.1}Fs_{9.2}$ for augite. On a pyroxene quadrilateral diagram (Fig. 6), NWA 2737 pyroxenes show a broad range of compositions similar to those of Chassigny pyroxenes (Fig. 6), along an elongated triangle following tie-lines of Fe–Mg equilibrium among Ca-rich and Ca-poor pyroxenes, which are nearly perpendicular to the two-pyroxene

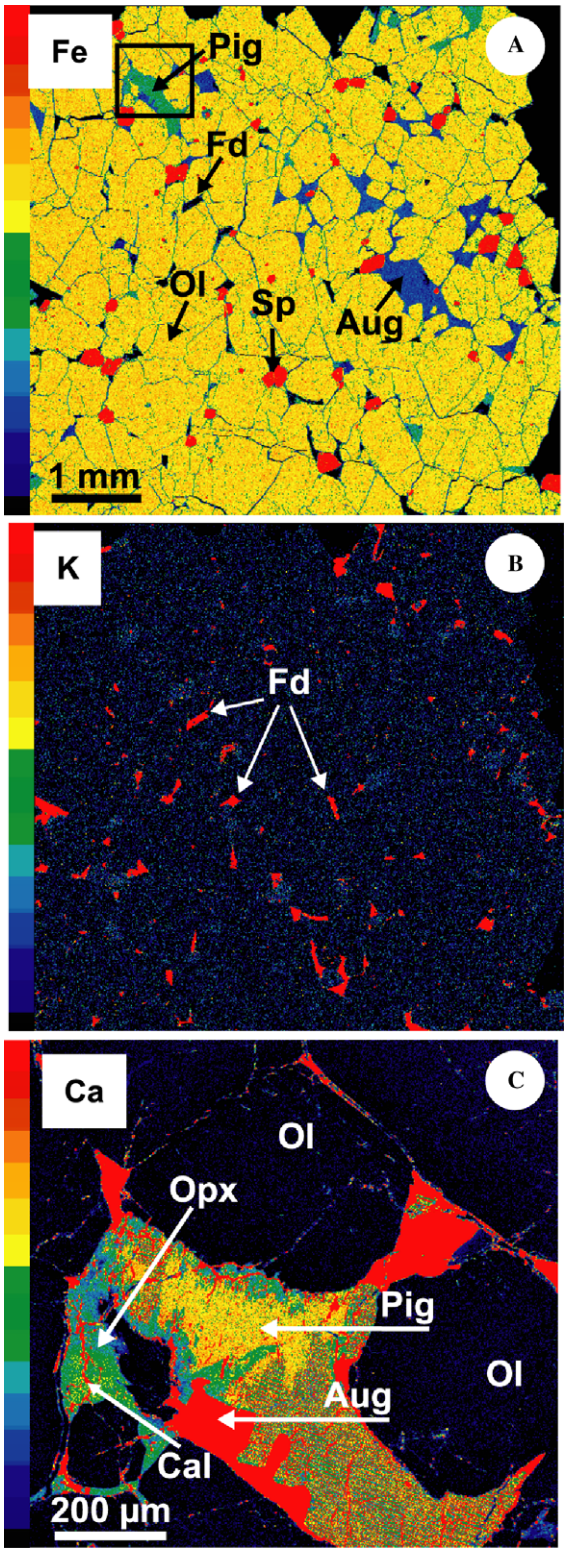

Fig. 2. (A) Fe chemical map of a section of the NWA 2737 meteorite showing the major mineralogy of the meteorite and the textural relationships among minerals: Aug, augite; Ol, olivine; Pig, pigeonite; Sp, spinel; Fd, K rich feldspar. (B) K chemical map of the same area revealing the presence of K rich feldpsar (Fd). (C) Enlarged view of interstitial coexisting pyroxenes (Ca chemical map). Three pyroxenes are identified by their chemical composition and their Raman spectra (shown on Fig. 4): augite, pigeonite, and orthopyroxene. Cal, calcite-rich vein; Opx, orthopyroxene.

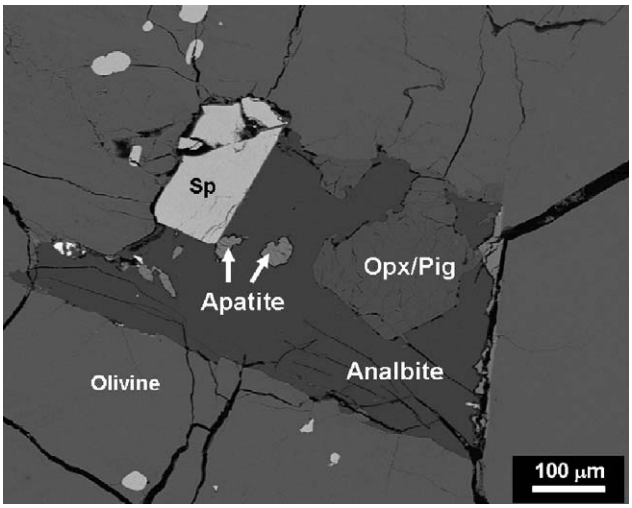

Fig. 3. Backscattered electron image of a section of NWA 2737 showing a feldspathic area, of analbite composition, between olivine crystals. The texture suggests late stage crystallization of the feldspar, which has been subsequently transformed into glass by shock. Associated minerals are: Ol, olivine; Sp, spinel; Aug, augite; Opx, orthopyroxene and apatite.

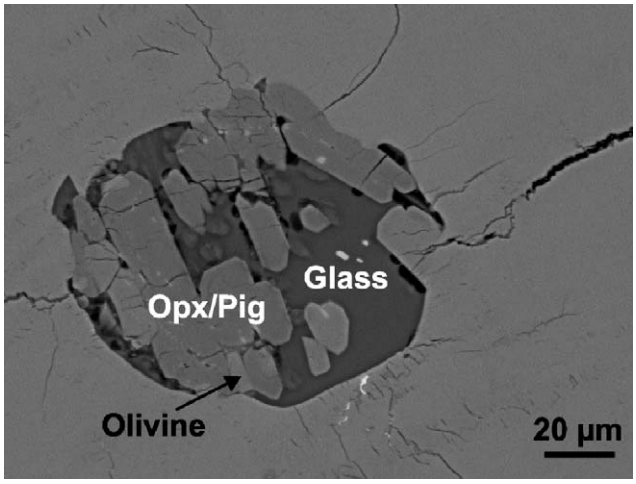

Fig. 4. Backscattered electron image of a melt inclusion in an olivine crystal. Prismatic low-Ca pyroxenes (Opx/Pig) and olivines (Ol) are embedded in a K–Na–Al–rich glass. Small bright crystallites of spinel are visible in the inclusion.

equilibrium isotherms (Lindsley, 1983). This trend is likely to be the result of buffering of the Fe–Mg ratio through equilibration with the dominant olivine phase.

In NWA 2737, spinel is found either as idiomorphic crystals occurring in the interstices or as anhedral grains enclosed in olivine. Both types show similar zoning trends, with a typical magmatic increase in Al, Fe, and Ti concentrations, and decrease in Cr abundances, from core to rim (from $Cr_{83.4}Uv_{3.6}Sp_{13.0}$ to $Cr_{72.0}Uv_{6.9}Sp_{21.1}$ for idiomorphic crystals). The range of chemical composition of spinels in NWA 2737 is much greater than in Chassigny (Fig. 7). The calculated Fe^{3+} content increases from core (~3 wt% Fe_2O_3) to rim (>8 wt% Fe_2O_3), which is also in agreement with magmatic zoning. Chemical profiles at the rims of idiomorphic chromite are consistent with possible diffusive re-equilibration with olivine over a few microns (in the case of Cr, Fe, and Mg), and no re-equilibration at all with pyroxenes.

A method for determining the magmatic f_{O_2} was recently proposed and is based on the change of the vanadium valence with oxygen fugacity (Papike et al., 2004). The V/(Cr + Al) ratio per formula unit in spinels in rocks originating from diverse parent body appears to be correlated with f_{O_2} (Papike et al., 2004). This ratio differs to some extent in spinels of NWA 2737 (0.28) and Chassigny (0.77) (Chassigny mineral data from Floran et al., 1978), indicating distinct oxidation conditions ($f_{O_2} = +0.6$ for NWA 2737 and $f_{O_2} = -1.3$ for Chassigny, relative to QFM). This oxy-barometer reveals oxidizing conditions, at least with respect to the whole set of f_{O_2} estimates available for martian meteorites (Goodrich et al., 2003; Herd et al., 2002; Wadhwa, 2001).

The feldspar in NWA 2737 is analbite (Fig. 2B) with the composition of $An_{1–13}Ab_{68–79}Or_{15–23}$, which is more restricted than that of the Chassigny alkali feldspar (Fig. 8). In Chassigny, plagioclase is present as an intercumulus phase. Plagioclase has not been observed in NWA 2737.

In some magmatic inclusions in olivine, a Ti-rich (up to 7 wt%) and F-rich (up to 3 wt%) silicate is observed. Both Ti and F enrichments suggest an amphibole of the kaersutite family. However the mineral is Ca-poor and enriched in Mg compared to what is expected for a kaersutite. In Chassigny, true kaersutites are encountered and they are poorer in F than the present mineral. Additional characterization of this phase is needed to determine whether it is indeed a (Mg, Fe)-rich member of the kaersutite amphibole group. Inclusions also contain a significant amount of Al-, K-, and Na-rich silicate glass.

Apatites in NWA 2737, like those in Chassigny, contain up to 2.7 wt% Cl. Fe-deficient pyrrhotite is the only sulfide encountered in the studied sections of NWA 2737. Calcium and magnesium carbonates have been described in the Chassigny fall (Wentworth and Gooding, 1994). In NWA 2737, carbonates are observed in two settings. They occasionally fill the interstices between olivines crystals. They are also found in cracks running throughout olivine or pyroxene crystals. In some cases, the carbonate-filled cracks are cut by the deformation features and fractures related to the shock which has affected the meteorite (Fig. 9). Calcite is the dominant carbonate but in some areas aragonite is found, as demonstrated by Raman spectra (Fig. 5). It seems likely that multiple generations of carbonates are present, but whether they are of terrestrial or martian origin is not clear. Textural evidence indicating pre-existence relative to shock features suggests a martian origin for at least some of them.

Table 1
Representative electron microprobe analyses of mineral phases

	SiO_2	TiO_2	Al_2O_3	Cr_2O_3	FeO	MnO	MgO	CaO	Na_2O	K_2O	P_2O_5	F	Cl	NiO	Total	End members
Olivine																
Mean	38.58	0.02	0.04	0.04	19.74	0.37	41.19	0.11	0.02	0.01	0.03	n.d.	n.d.	0.09[a]	100.22	$Fo_{79.0}$
σ ($n = 292$)	*0.56*	*0.03*	*0.09*	*0.08*	*1.29*	*0.09*	*1.00*	*0.12*	*0.05*	*0.01*	*0.04*	—	—	0.04[a]	—	
Low-Fe	38.85	0.02	0.08	0	18.97	0.44	41.23	0.03	0.02	0.005	0	n.d.	n.d.	0.2	99.85	$Fo_{79.5}$
High-Fe	38.93	0.03	0.06	0	19.69	0.32	40.59	0.12	0.04	0	0.02	n.d.	n.d.	n.d.	99.83	$Fo_{78.6}$
Orthopyroxene																
Mean	55.39	0.27	0.6	0.27	12.57	0.4	29.1	1.72	0.05	n.d.	0.01	0.09	n.d.	n.d.	100.47	$En_{77.8}Wo_{3.3}Fs_{18.9}$
σ ($n = 14$)	*0.52*	*0.15*	*0.19*	*0.11*	*0.37*	*0.07*	*0.49*	*0.52*	*0.04*	—	*0.04*	*0.11*	—	—	—	
Low-Fe	55.08	0.5	0.5	0.08	12.54	0.33	29.42	1.4	0.04	0.022	n.d.	n.d.	—	—	99.93	$En_{78.5}Wo_{2.7}Fs_{18.8}$
High-Fe	55.59	0.13	0.45	0.23	13.28	0.55	28.27	1.64	0.04	0.002	n.d.	—	—	—	100.18	$En_{76.6}Wo_{3.2}Fs_{20.2}$
Pigeonite																
Mean	54.95	0.14	0.53	0.41	11.44	0.35	26.19	5.52	0.16	n.d.	0.01	0.13	n.d.	n.d.	99.72	$En_{71.6}Wo_{10.8}Fs_{17.5}$
σ ($n = 7$)	*0.29*	*0.03*	*0.11*	*0.11*	*0.98*	*0.08*	*1.11*	*2.25*	*0.05*	—	*0.03*	*0.16*	—	—	—	
Low-Ca	55.31	0.12	0.46	0.49	12.16	0.36	27.06	4.11	0.16	n.d.	n.d.	—	—	—	100.24	$En_{73.5}Wo_{8.0}Fs_{18.5}$
High-Ca	54.01	0.16	0.84	0.67	9.01	0.44	23.29	11.2	0.3	0.018	0.007	—	—	—	100.02	$En_{64.0}Wo_{22.1}Fs_{13.9}$
Augite																
Mean	53.06	0.26	1.00	0.89	6.76	0.25	18.31	18.55	0.30	0.01	0.01	0.09	n.d.	n.d.	99.49	$En_{51.7}Wo_{37.6}Fs_{10.7}$
σ ($n = 25$)	*0.55*	*0.05*	*0.25*	*0.15*	*0.30*	*0.10*	*0.35*	*0.20*	*0.05*	*0.02*	*0.02*	*0.15*	—	—	—	
Low-Ca	53.79	0.25	0.85	0.55	8.07	0.27	19.53	16.33	0.26	n.d.	n.d.	n.d.	—	—	99.90	$En_{54.6}Wo_{32.8}Fs_{12.6}$
High-Ca	52.93	0.36	1.15	1	5.79	0.3	16.42	21.57	0.52	n.d.	n.d.	—	—	—	100.04	$En_{46.7}Wo_{44.1}Fs_{9.2}$
Feldpsar																
Mean	65.26	0.14	20.59	0.04	0.54	0.03	0.02	1.62	8.42	3.18	0.02	0.16	0.02	0.04	100.07	$An_{7.8}Ab_{73.8}Or_{18.4}$
σ ($n = 18$)	*1.15*	*0.08*	*0.81*	*0.04*	*0.21*	*0.04*	*0.04*	*0.64*	*0.76*	*0.42*	*0.04*	*0.25*	*0.04*	*0.04*	—	
High-Na	65.83	0.21	20.00	0.10	0.34	n.d.	n.d.	1.53	8.96	2.94	n.d.	0.35	n.d.	0.10	100.35	$An_{7.2}Ab_{76.3}Or_{16.5}$
Low-Na	67.71	0.12	20.36	0.08	0.56	n.d.	n.d.	0.91	6.73	3.64	n.d.	0.13	—	—	100.25	$An_{5.2}Ab_{69.9}Or_{24.9}$
K–Na rich glass[b]																
Mean	76.26	0.17	11.96	0.61	0.44	0.02	0.60	0.10	3.09	3.40	0.02	0.07	0.10	—	96.84	Qz 45 Or 20 Ab 26 An 1[c]
σ ($n = 6$)	*1.41*	*0.01*	*0.60*	*0.23*	*0.34*	*0.04*	*1.64*	*0.11*	*0.94*	*0.27*	*0.02*	*0.11*	*0.05*	—	—	
High-Na	75.12	0.18	12.99	0.97	0.52	n.d.	0.03	0.31	4.79	3.52	0.01	0.15	0.07	—	98.67	Qz 33 Or 21 Ab 40 An 2[c]
Low-Na	76.91	0.16	11.21	0.72	0.29	n.d.	0.05	0.04	2.80	3.80	0.01	n.d.	0.02	—	96.01	Qz 46 Or 22 Ab24 An 0[c]
Kaersutite																
Low-F	39.80	6.40	12.97	0.92	11.26	0.06	19.40	0.54	1.87	5.29	0.05	1.89	0.18	0.08	100.72	
High-F	38.15	7.52	14.30	1.23	11.11	0.22	18.35	1.12	2.52	3.62	0.01	3.00	0.31	n.d.	101.46	
Spinel																
Mean core	0.01	1.30	6.39	57.55	28.14	0.45	5.74	0.01	0.01	0.003	0.01	n.d.	n.d.	n.d.	99.61	$Cr_{82.8}Uv_{3.5}Sp_{13.7}$
σ ($n = 10$)	*0.02*	*0.09*	*0.35*	*0.44*	*0.57*	*0.16*	*0.22*	*0.03*	*0.03*	*0.01*	*0.02*	—	—	—	—	
High-Cr	0.002	1.32	6.13	58.46	27.79	0.36	5.67	n.d.	n.d.	n.d.	n.d.	—	—	—	99.73	$Cr_{83.4}Uv_{3.6}Sp_{13.0}$
Low-Cr	n.d.	2.48	9.63	48.93	32.57	0.47	5.52	0.04	n.d.	n.d.	0.02	—	—	—	99.64	$Cr_{72.0}Uv_{6.9}Sp_{21.1}$
Apatite																
Mean	1.02	0.02	0.32	0.02	0.77	0.06	0.47	53.42	0.2	0.02	41.54	1.36	2.68	0.08	100.5	
σ ($n = 14$)	*0.86*	*0.04*	*0.41*	*0.04*	*0.37*	*0.04*	*0.30*	*1.42*	*0.11*	*0.04*	*1.50*	*0.75*	*0.75*	*0.04*	—	

Unit is wt% except for the end members compositions (mol %).
n.d. = not detected; σ, standard deviation.
[a] NiO content was measured for 29 analyses only.
[b] Glass inclusion in chromite.
[c] CIPW Norm.

6. Shock features

There are many features observed in NWA 2737 that can be attributed to shock. Olivines, although they are rich in Mg ($Fo_{78.5}$), are dark and this gives a black appearance to the stone. Black forsteritic olivine exists in terrestrial rocks, and is believed to be produced by high-temperature oxidation (Putnis, 1979). However, none of the expected products (magnetite and hypersthene) usually associated to this process have been observed in the present study. Most dark olivine grains display alternate black and colorless parallel zones and exhibit unusual sets of perpendicular planar defects (Fig. 10). High-resolution images (Fig. 11) obtained on these black olivine grains show zones in which the lattice atomic planes are corrugated. The Raman spectra of the black olivines are different from those of usual magmatic or metamorphic olivines, and of the limited areas of colorless olivines in NWA 2737 (Fig. 5). The low wave

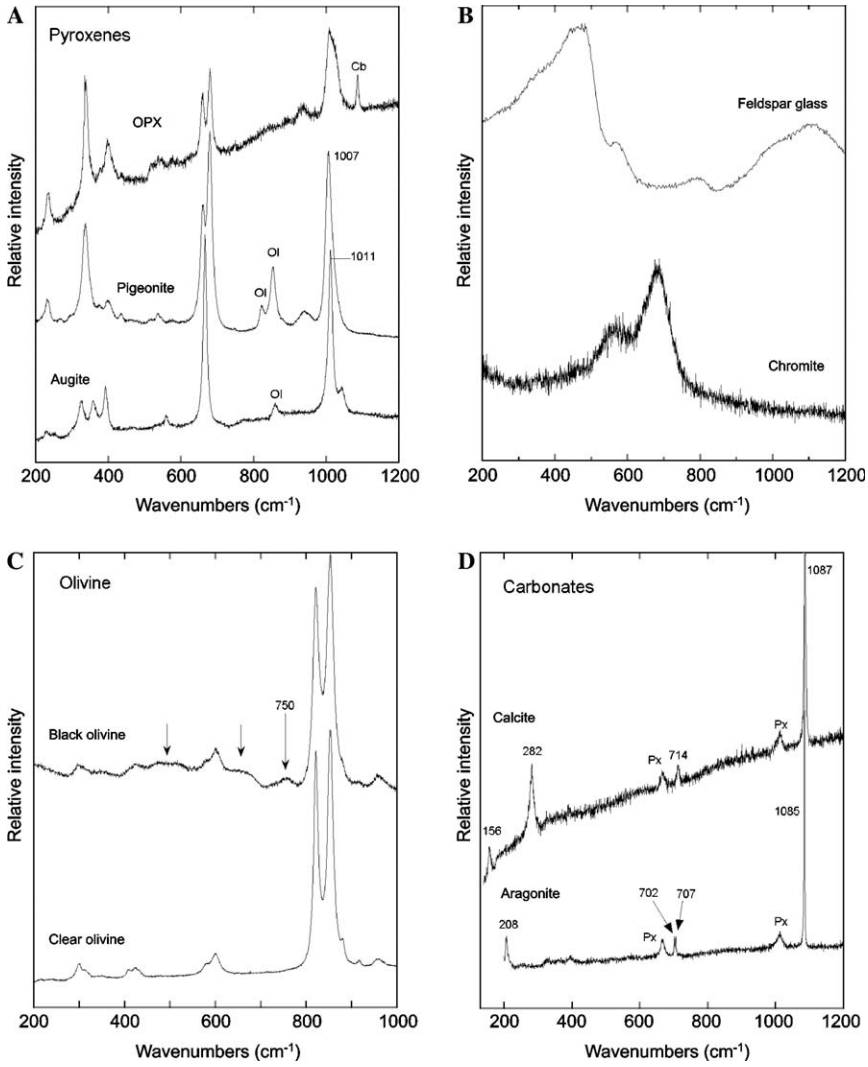

Fig. 5. Raman spectra of the major phases in NWA 2737. (A) Raman spectra of pyroxenes. The spectra were recorded on the area shown in Fig. 1C and demonstrate the presence of three pyroxenes in contact with the olivine. Low-Ca pyroxenes (Orthopyroxene (Opx) and pigeonite) are characterized by the presence of a doublet near 660 and 680 cm^{-1} while the augite spectrum has a single peak at 667 cm^{-1}. The difference between pigeonite and Opx is marked by a strong dissymmetry of the high frequency peak near 1010 cm^{-1} (Huang et al., 2000). In the Opx spectrum, a strong Raman peak for calcite is observed, consistent with the presence of calcite veinlets in this area (see Fig. 1C). (B) Typical Raman spectrum of glass of analbite composition. Also shown is the Raman spectrum of a spinel. (C) Raman spectra of olivines. The lower spectrum is obtained on the colorless area (see Fig. 10A). The spectrum shows only the expected vibrations of well-crystallized and unshocked olivine. The upper spectrum is characteristic of the majority of olivines in NWA 2737. In addition to the diagnostic olivine peaks (lower spectra), several broad bands are present (510, 660, and 750 cm^{-1}). The 510 and 660 cm^{-1} bands are commonly observed in defect-rich olivines. The 750 cm^{-1} band is unusual and could correspond to the presence of Si–O–Si bridges as found in the $(Mg,Fe)_2SiO_4$ wadsleyite (McMillan and Akaogi, 1987). (D) Raman spectra of calcite and aragonite encountered in the numerous fractures running throughout the section of NWA 2737 studied here.

number peaks are broader and an additional band close to 750 $cm^{-1}$is observed in the black areas when compared with the colorless areas. The additional observed mode is consistent with the building of Si–O–Si bridges such as those of $(Mg,Fe)_2SiO_4$-wadsleyite, the high-pressure polymorph of olivine which has already been observed in the Chassigny meteorite by TEM studies (Malavergne et al., 2001). Broadening of peaks and appearance of new bands is consistent with the observed lattice distortions at the atomic scale. The deformation of lattice planes observed in the TEM studies may be due to a hindered transformation to wadsleyite, suggesting it is produced by shock. Such deformation may affect the absorption properties of crystals, by favoring charge transfer for instance, and is likely responsible for the color of olivines. The colorless olivine areas could have resulted from the re-crystallization of olivine that was partially melted during the shock event, as previously suggested for Chassigny (Langenhorst and Greshake, 1999). A detailed transmission electron microscopic survey is needed to confirm this hypothesis.

Grains with analbite compositions display Raman spectra typical of glass (Fig. 5). This is attributed to the transformation of magmatic feldspar into maskelynite during the shock. The absence of melt pockets or shock melt veins

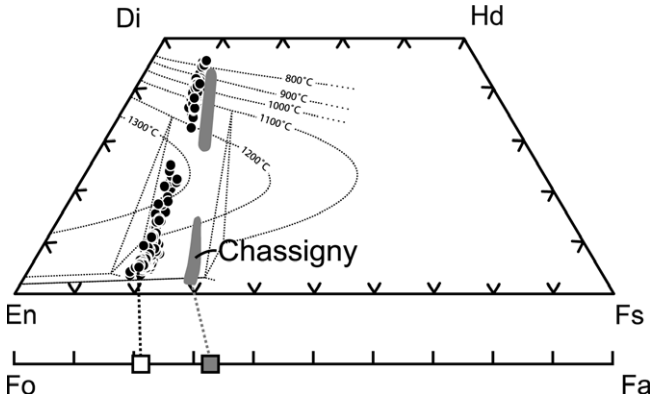

Fig. 6. Major element compositions of pyroxenes and olivines in NWA 2737 (solid circles and solid square). The range of compositions for these minerals in the Chassigny meteorite (grey areas and grey square) is also shown for comparison (Floran et al., 1978). The dashed curves are the calculated isotherms for equilibrium relationships between coexisting pyroxenes in the Wo–Fs–En system (Lindsley, 1983).

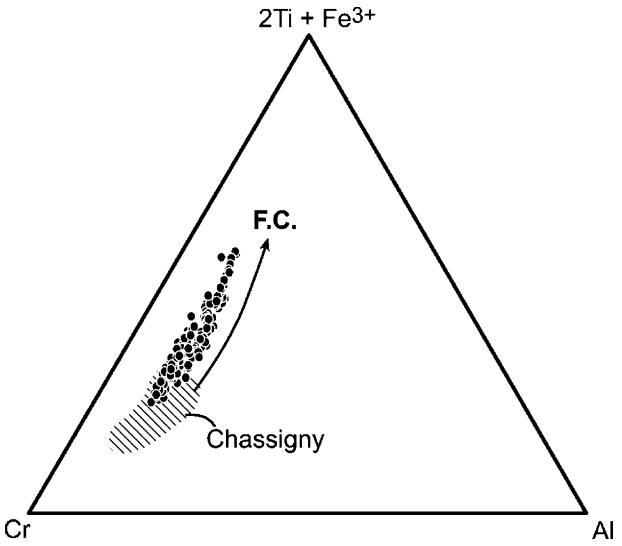

Fig. 7. Cr-Al-2Ti + Fe^{3+} plot (atomic %) of spinel in NWA 2737 and Chassigny (dashed area, from Floran et al., 1978). The curved arrow indicates the typical evolution of spinel composition during closed-system fractional crystallization (FC). The chemical composition of spinels in NWA 2737 records a large degree of magmatic evolution.

containing high-pressure phases hinders quantitative estimation of the P–T shock conditions.

7. Chemistry

As expected from the compositions and the proportions of the various phases, the major element abundances in NWA 2737 are dominated by olivine. NWA 2737 and Chassigny display similar bulk compositions, with the exception of Fe and Mg: NWA 2737 is significantly richer in MgO (37 versus 32 wt%) (Table 2), as also illustrated by the higher Mg# of olivine and pyroxenes.

Many weathered hot-desert meteorite finds display strong enrichments in U, Sr, and Ba (e.g., Barrat et al., 2003; Crozaz et al., 2003, and references therein). In the case of NWA 2737, the Ba and Sr abundances are low. This suggests that the effects of terrestrial residence are negligible, or at least extremely limited for the trace elements analyzed here. Indeed, the Sr/Nd, Ba/Th, and U/Th ratios in NWA 2737 are similar to those determined in Chassigny (e.g., Mason et al., 1975; Nakamura et al., 1982a), which was recovered just after its fall, and thus not subjected to any significant terrestrial alteration. Also, Sr isotopic data for NWA 2737 indicates that a substantial fraction of its Sr

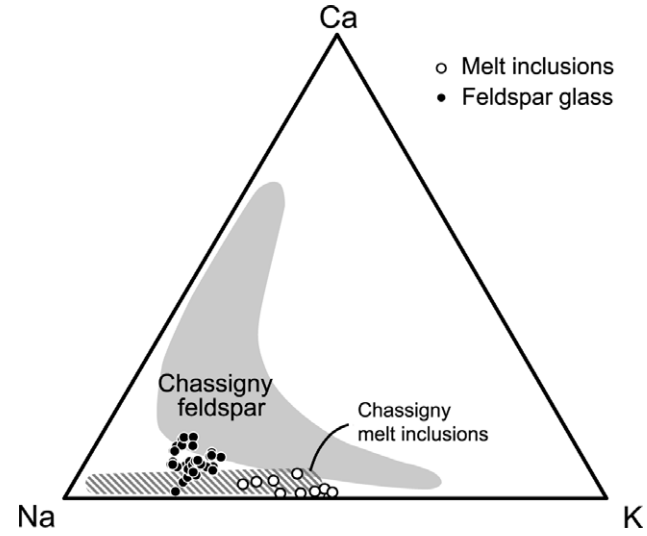

Fig. 8. The compositions of maskelynite (filled circles) and melt inclusion glass (open circles) in NWA 2737 on a Ca–Na–K triangular plot (molar proportions). For comparison, the compositional range of Chassigny maskelynites is indicated (grey area) as well as glasses from melt inclusions in Chassigny (dashed area). The data for Chassigny are taken from (Floran et al., 1978). Unlike in Chassigny, maskelynites with compositions on the albite-anorthite join are absent in NWA 2737.

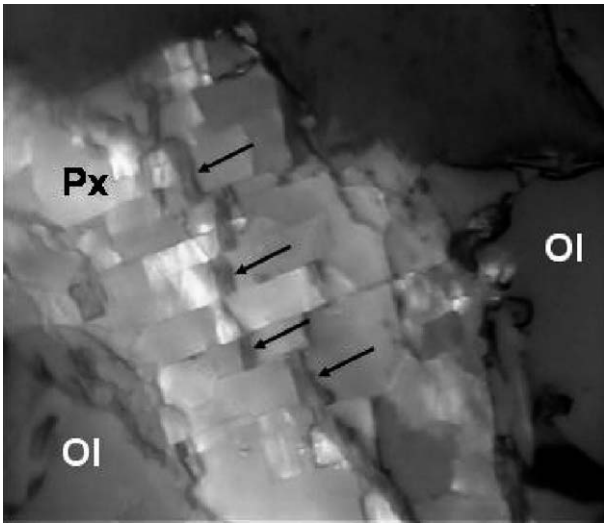

Fig. 9. Reflected light image of a possible pre-terrestrial (martian) calcite vein in NWA 2737 (black arrows). The parallel shock-induced fractures crossing the pyroxene crystal (Px) have clearly dislocated the carbonate vein, and post-date calcite formation.

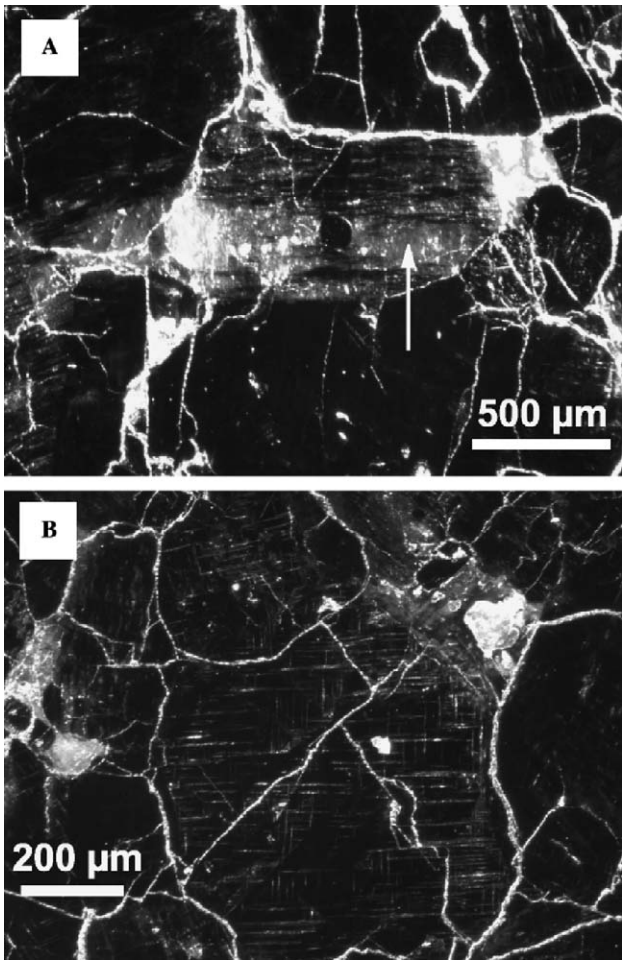

Fig. 10. Shock textures in olivines. The images were obtained under a binocular microscope with oblique illumination of the thick section with white light. (A) In some rare areas, the dark olivines show broad colorless stripes (arrow). The Raman spectra of black olivines exhibit the vibrational modes of olivine as well as additional bands. Raman spectra (Fig. 4) recorded on this colorless stripe show that it corresponds to undeformed and untransformed olivine, probably reflecting shock-induced melting and subsequent recrystallization. (B) The central olivine grain shows a typical network of perpendicular fractures visible under the binocular microscope. Among the martian meteorites, this macroscopic deformation of olivine crystals appears to be a feature unique to NWA 2737.

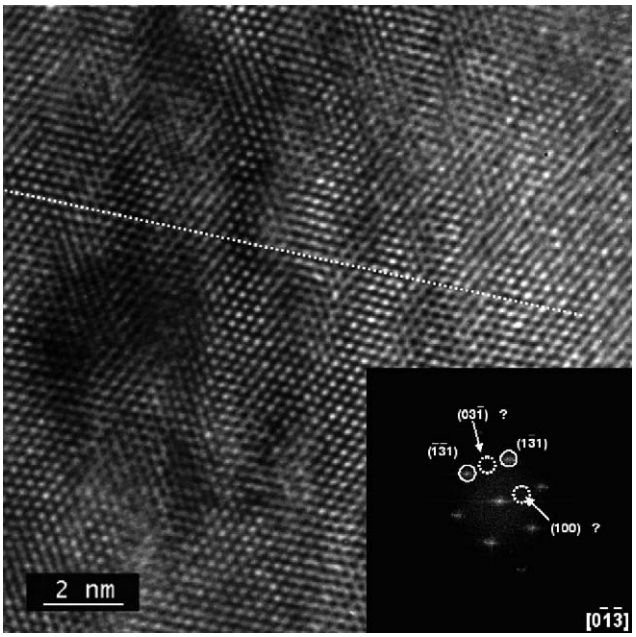

Fig. 11. High resolution T.E.M. images of the olivine lattice in a dark olivine from NWA 2737. The atomic lattice shows alternating clear and dark grey areas corresponding to distinct orientations of the atomic lattice. The atomic positions do not correspond to a straight line (as indicated by the dashed line), but rather show an undulating pattern, most likely resulting from shock. Fast Fourier Transform of the HRTEM image is only approximately indexed when using the [0$\bar{1}\bar{3}$] zone axis (with orthorhombic cell parameters as given by Birle et al. (1968): $a = 0.4762$ nm, $b = 1.0225$ nm, $c = 0.5994$ nm), and the (100) and (0$\bar{3}$1) spots are extinct.

is of terrestrial origin (Misawa et al., 2005), thereby suggesting that the pre-terrestrial Sr abundance in this meteorite was lower than ~20–25 ppm. As such, heterogeneous terrestrial alteration of this meteorite cannot be ruled out. In any case, the level of terrestrial contamination in the aliquots of NWA 2737 analyzed here is likely to be rather low, and we argue that the trace element abundances reported here (excepted Sr and Ba) have not been significantly modified during terrestrial residence. When compared with Chassigny, NWA 2737 is richer in Ni and has higher concentrations of the most incompatible trace elements (e.g., Zr, Nb, Rb, and the light REE). The difference in Ni abundance is explained by a more primitive composition of the NWA 2737 parental melt, as also suggested by the higher Mg# of the olivine and pyroxene cores. The higher trace element abundances compared to Chassigny may be due to a higher proportion of incompatible element rich interstitial phases such as apatite in the aliquot of NWA 2737 analyzed here (which may or may not be representative of the true whole rock). Nevertheless, similarities in the trace element abundance patterns in bulk samples of these two chassignites underscore their similar petrogenetic histories (Fig. 12). Normalized trace element abundance patterns for both meteorites are characterized by a light REE enrichment, U spikes, negative Hf anomalies, and low Rb concentrations. The same features are shared by the nakhlites, which have similar crystallization ages (Misawa et al., 2005; Nyquist et al., 2001), and whose mantle sources were probably similar.

NWA 2737 displays a light REE enrichment more pronounced than Chassigny ($(La/Sm)_n = 2.77$ and 1.71, respectively, for NWA 2737 and Chassigny), and a small negative Eu anomaly ($Eu/Eu* = 0.88$) unlike Chassigny ($Eu/Eu* = 1.00$, Nakamura et al., 1982b). Moreover, the Chassigny whole rock exhibits a slightly concave heavy REE pattern that is not observed in NWA 2737. These differences are significant, but do not necessarily imply that these rocks formed from unrelated parental melts. In the case of dunitic cumulates, it is well known that the REE budget of the whole rocks can be controlled by the abun-

Table 2
Major (wt%) and trace element (in ppm) abundances in NWA 2737

SiO_2	37.0	(a)
TiO_2	0.13	(a)
Al_2O_3	0.86	(a)
Cr_2O_3	1.71	(a)
Fe_2O_3	21.79	(a)
MnO	0.4	(a)
MgO	37.1	(a)
CaO	0.84	(a)
Na_2O	0.17	(a)
K_2O	0.05	(a)
P_2O_5	0.10	(a)
Total	100.15	
V	*70*	(a)
Ni	875	(a)
Sc	4.6	(b)
Co	78	(b)
Cu	4.3	(b)
Zn	45	(b)
Ga	1.43	(b)
Rb	1.28	(b)
Sr	27.2	(b)
Y	1.21	(b)
Zr	5.01	(b)
Nb	1.19	(b)
Mo	0.15	(b)
Cs	0.063	(b)
Ba	37.5	(b)
La	1.17	(b)
Ce	2.87	(b)
Pr	0.363	(b)
Nd	1.43	(b)
Sm	0.266	(b)
Eu	0.0721	(b)
Gd	0.237	(b)
Tb	0.0367	(b)
Dy	0.213	(b)
Ho	0.0427	(b)
Er	0.117	(b)
Yb	0.105	(b)
Lu	0.017	(b)
Hf	0.14	(b)
Ta	0.07	(b)
W	0.10	(b)
Pb	0.46	(b)
Th	0.13	(b)
U	0.056	(b)

(a) = ICP–AES; (b) = ICP–MS.

dances of accessory phases. Wadhwa and Crozaz (1995) have shown that the REE (particularly, the light REE) budget of Chassigny is strongly dominated by apatite and slight differences in the abundance of this late-stage interstitial mineral can affect the REE abundances and patterns of different bulk samples of this meteorite.

The REE concentrations in individual minerals of NWA 2737 were determined to evaluate their impact on the REE budget of the whole rock, to help constrain the petrogenetic history and to provide a comparison with Chassigny. Representative REE abundances in various minerals are given in Table 3 and illustrated in Fig. 13. It is evident from these data that apatite is the main REE carrier in NWA 2737, as is the case in Chassigny (Wadhwa and Crozaz, 1995). This mineral accounts for nearly all the light LREE, about 75% of Sm and about 15% of Yb, while the remaining REE are located in the silicates. The REE patterns of pyroxenes, olivine, and phosphates in NWA 2737 are similar to those of minerals in Chassigny (Fig. 13). Although the major element compositions of the feldspars in NWA 2737 and Chassigny are different, their REE patterns are quite similar. The striking resemblances between the REE patterns of the phases of both chassignites suggest that these rocks were formed from parental melts characterized by similar REE patterns.

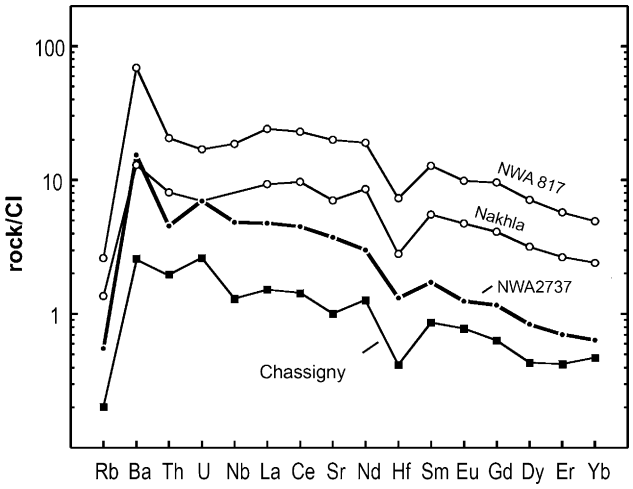

Fig. 12. Trace element abundances in a bulk sample of NWA 2737 (this study). For comparison, abundances in bulk samples of Chassigny (Mason et al., 1975; Nakamura et al., 1982a), and the nakhlites Nakhla (Nakamura et al., 1982b) and NWA 817 (Sautter et al., 2002) are also shown. All trace element abundances shown here are normalized to the chondritic values of Sun and McDonough (1989).

The ion microprobe trace element data also demonstrate that magmatic zoning is preserved in the augites of NWA 2737. The REE abundances are twice as high in the augite rim as in the core. In addition to the REE, concentrations of Y and Zr were also determined in this mineral, and these correlate with each other and with the REE abundances (Fig. 14). Thus, REE and other trace element abundances in pyroxenes in NWA 2737 and Chassigny have not been affected by subsolidus equilibration, and provide a robust record of the crystallization history. The overall similarity of the pyroxene zoning trends in NWA 2737 and Chassigny (Figs. 13 and 14) additionally support similar petrogenetic histories and parental melt REE compositions for these two chassignites. We note that the somewhat narrower range of REE and other trace element abundances in pyroxenes of NWA 2737 compared to Chassigny (Fig. 14) may be a sampling artifact.

Determination of trace element abundances in the parental melt of a cumulate is a difficult task (e.g., James et al., 2002; Barrat, 2004; and references therein). Given that pyroxenes in NWA 2737 have retained their original magmatic REE zoning, and since these are some of the earliest crystallizing REE-bearing minerals in the chassignites, the melt in equilibrium with the pyroxene core should re-

Table 3
Representative REE abundances in minerals of NWA 2737 measured by ion probe (in ppm)

	La	Ce	Pr	Nd	Sm	Eu	Gd	Tb	Dy	Ho	Er	Tm	Yb	Lu
Augite (core)	0.65	2.75	0.51	2.83	0.92	0.22	1.07	0.18	1.02	0.21	0.57	0.07	0.43	0.05
Augite (rim)	1.47	6.50	1.41	7.21	2.33	0.54	2.62	0.34	2.34	0.46	1.11	0.14	0.86	0.09
Low Ca pyroxene	0.068	0.240	0.033	0.175	0.077	0.025	0.127	0.029	0.212	0.045	0.153	0.026	0.164	0.032
Olivine	0.003	0.004	0.002	0.006	0.007	b.d.	b.d.	0.003	0.030	0.009	0.044	0.011	0.089	0.015
Feldspar	2.46	3.40	0.27	0.51	0.05	0.59	0.02	b.d.	b.d.	b.d.	b.d.	b.d.	b.d.	b.d.
Apatite grain1	302	666	73	254	38	17.2	40	7.5	24.0	3.80	12.59	1.25	3.28	0.59
Apatite grain 2	689	1597	180	676	100	18.9	93	18	65	10.08	25.2	2.88	7.14	0.20

b.d. = below detection.

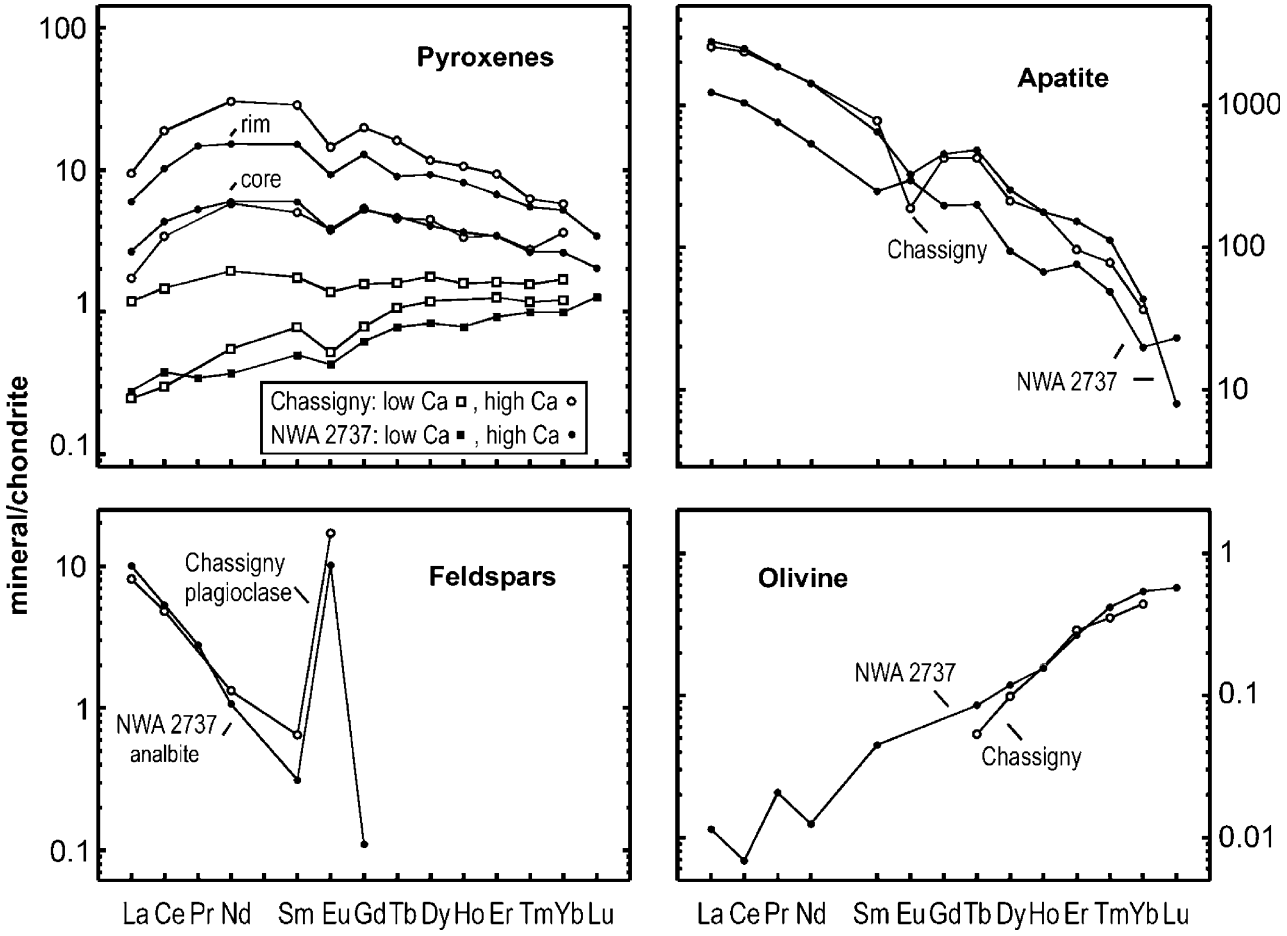

Fig. 13. REE abundances in NWA 2737, normalized to the CI chondrite values of Evensen et al. (1978). Data for Chassigny minerals from Wadhwa and Crozaz (1995) are shown for comparison.

flect the composition of the parental melt. Therefore, we have estimated the REE compositions of the melts in equilibrium with the pigeonite and the augite cores using appropriate mineral/melt partition coefficients (Fig. 15). The partition coefficients we have utilized for this purpose are those obtained by McKay et al. (1986) for pyroxenes containing 12% and 36% wollastonite (for pigeonite and augite, respectively). The estimated melt in equilibrium with the core of the NWA 2737 augite displays a REE pattern that parallels that of the bulk rock at ~80 × CI for Ce and 10 × CI for Yb. Ce and Yb abundances calculated in the melt in equilibrium with the low-Ca pyroxene are similar, although the estimated Nd, Sm, and Gd abundances are somewhat different from those estimated in the melt in equilibrium with the augite. This is most likely due to the fact that the abundance of the light REE in the low-Ca pyroxene are significantly lower than in the augite, and the corresponding uncertainties in these data are higher, such that estimated light REE pattern of the parental melt based on the low-Ca pyroxene composition is not as certain as that based on the augite core composition. Analogous results are obtained using the Chassigny pyroxene

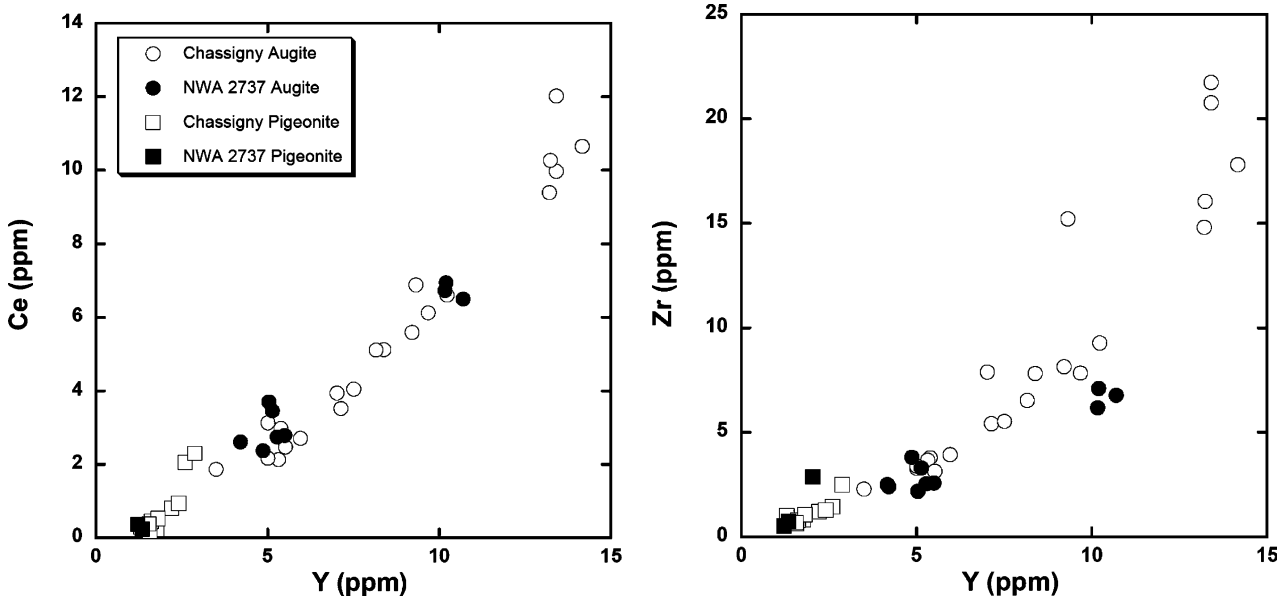

Fig. 14. Ce and Zr concentrations versus Y abundances in pyroxenes of NWA 2737. Data for Chassigny pyroxenes from Wadhwa and Crozaz (1995) are shown for comparison.

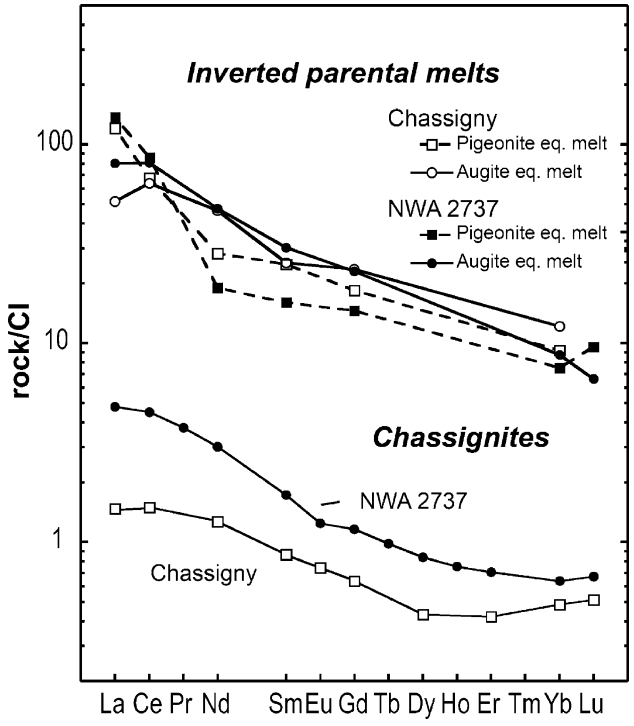

Fig. 15. Estimated REE abundances in melts in equilibrium with pyroxenes of NWA 2737. For comparison, melts in equilibrium with pyroxenes of Chassigny are also shown (REE data for Chassigny pyroxenes from Wadhwa and Crozaz, 1995). Also shown are the whole rock REE patterns for NWA 2737 (this study) and Chassigny (Nakamura et al., 1982a). All REE abundances shown here are normalized to the CI chondrite values of Evensen et al. (1978).

compositions and confirm that both chassignites formed from parental melts displaying a very similar degree of light REE enrichment.

8. Petrogenesis of NWA 2737 and general discussion

NWA 2737 is a martian dunite (~90 wt% olivine) that is petrographically and chemically similar to Chassigny. This meteorite is classified as the second chassignite. However, there are some slight but notable differences between them.

The two chassignites formed from olivine and chromite accumulation. Although the modal abundance of olivine is almost the same in both meteorites, the Mg# is distinct in the two stones (Mg# is 78.5 in olivine of NWA 2737, while it is 69 in olivine of Chassigny). This difference suggests that the parent melt from which Chassigny olivines were formed was more evolved than that of NWA 2737. The REE abundances in mineral phases indicate that the two chassignites formed from melts displaying a similar degree of LREE enrichment. Nd isotopic systematics are compatible with the proposed petrogenetic relationship between the two chassignites (Misawa et al., 2005), possibly through olivine fractionation from the parental melt.

Unlike Chassigny, plagioclase is absent from NWA 2737 and only analbite is observed. The composition of analbite in NWA 2737 is more restricted than that of alkaline feldspars in Chassigny (Fig. 7). Because Ca, Na, and K are incompatible with the two cumulus phases (olivine and spinel), the concentrations of these elements in the bulk rock should reflect their abundance in the crystallizing intercumulus liquid. The $CaO/(Na_2O + K_2O)$ ratio is similar in the two meteorites, with values of 4.40 for NWA 2737 and 3.90 for Chassigny. Therefore, the absence of plagioclase in NWA 2737 is neither due to depletion in Ca nor enrichment in the alkali elements. A lower Al concentration in the intercumulus liquid in NWA 2737 than in Chassigny may explain the absence of plagioclase, since this would induce the incorporation of Ca as a $CaSiO_3$ compo-

nent in pyroxene rather than as $CaAl_2Si_2O_8$ in feldspar. This is consistent with the lower Al content in NWA 2737 pyroxenes compared to Chassigny pyroxenes (Floran et al., 1978). Further study of NWA 2737 melt inclusions will be required to constrain the major element composition of NWA 2737 parental melt, as was previously done in the case of Chassigny (Johnson et al., 1991).

The cooling rate of chassignites can be tentatively used to infer their geological environment on Mars. The crystallization of the rock had to be fast enough to permit melt inclusion entrapment, but slow enough to enable diffusive equilibration of Fe–Mg in olivines and pyroxenes and the development of exsolution features in pigeonite. In the opposite, the temperature inferred from the pyroxene-chromite thermometer is ~1011 °C, significantly lower than the crystallization temperature of these minerals in mafic systems, which reflects the absence of diffusive Fe–Mg exchange between the two minerals. Absolute cooling rates have previously been calculated from the re-equilibration of Ca between olivine and their magmatic inclusions or adjacent pyroxenes (Mikouchi et al., 2005; Monkawa et al., 2004). These studies yielded constant cooling rates of 28 °C/year for Chassigny (Monkawa et al., 2004) and 30 °C/year for NWA 2737 (Mikouchi et al., 2005). These values are consistent with a burial depth of a few tens of meters, consistent with formation of the chassignites within a thick lava flow or a shallow dyke.

The initial water content of martian magmas is a matter of debate (Beck et al., 2004a; Herd et al., 2005; Jones, 2004; McSween et al., 2001). Kaersutitic amphibole, which has a mineral structure capable of incorporating up to 2.5 wt% of H_2O (Hawthorne, 1981), has been described in melt inclusions in minerals in the shergottites and in Chassigny. Based on stoichiometric considerations and their low halogen contents, it was proposed that kaersutites in the martian meteorites were hydrous (Floran et al., 1978; Johnson et al., 1991; Treiman, 1985). As such, high water contents (0.2 wt% for Zagami and Shergotty (Treiman, 1985) and 1.5 wt% for Chassigny (Johnson et al., 1991)) were proposed for the melts trapped in the kaersutite-bearing inclusions, to allow saturation of hydrous-amphibole. Moreover, because of the low solubility of H_2O at low pressure, confining pressures above 1.5 kbar were suggested for the formation of melt inclusions (Johnson et al., 1991). However, ion microprobe analyses of kaersutites in the martian meteorites yielded low hydrogen abundances of ~0.1 wt% H_2O, an order of magnitude lower than was expected for purely hydrous kaersutite (Watson et al., 1994), thereby suggesting that the parental melts of these meteorites were anhydrous (or, if originally hydrous, had experienced substantial degassing prior to the formation of melt inclusions). In the case of NWA 2737, a silicate phase that could belong to the amphibole family has been detected. Structural formula calculations match the amphibole group, with the monovalent anion site being almost fully occupied by F^- and Cl^-, and with a minor amount of OH^- (Table 1). If this phase is indeed an amphibole, given the high solubility of halogens in basaltic liquid at low pressure (1 bar) (Carroll and Webster, 1994), its formation in the melt inclusions of NWA 2737 requires neither a high water content nor a high confining pressure.

Acknowledgments

Carine and Bruno Fectay generously provided the NWA 2737 sample. We thank Christian Koeberl for the editorial handling, Ahmed El Goresy and Harry McSween Jr for constructive comments. Access to the Washington University ion microprobe was possible through the kind courtesy of E. Zinner and C. Floss. The CLYME (Consortium Lyonnais de Microscopie Electronique) is gratefully acknowledged for the use of the TEM facilities and the GEMPPM (Groupe d'Etude de Métallurgie Physique et de Physique des Matériaux) for granting access to the SEM. Raman spectroscopy measurements were made on a INSU (Institut National des Sciences de l'Univers) national instrument. This work was partly supported by NASA Grant NAG5-12077 MW. P.B. thanks Hervé Bertrand for helpful discussions. This research made benefit of the Mars Meteorite Compendium compiled by Charles Meyer.

Associate editor: Christian Koeberl

References

Barrat, J.A., 2004. Determination of parental magmas of HED cumulates: the effects of interstitial melts. *Meteorit. Planet. Sci.* **39** (11), 1767–1779.

Barrat, J.A., Blichert-Toft, J., Gillet, P., Keller, F., 2000. The differentiation of eucrites: the role of in situ crystallization. *Meteorit. Planet. Sci.* **35** (5), 1087–1100.

Barrat, J.A., Jambon, A., Bohn, A., Blichert-Toft, J., Sautter, V., Göpel, C., Gillet, P., Boudouma, O., Keller, F., 2003. Petrology and geochemistry of the unbrecciated achondrite Northwest Africa 1240 (NWA 1240): an HED parent body impact melt. *Geochim. Cosmochim. Acta* **67** (20), 3959–3970.

Beck, P., Barrat, J.A., Chaussidon, M., Gillet, P., Bohn, M., 2004a. Li isotopic variations in single pyroxene from the Northwest Africa 480 (NWA 480) shergottite: a record of degassing of Martian magmas? *Geochim. Cosmochim. Acta* **68**, 2925–2933.

Birle, J.D., Gibbs, G.V., Moore, P.B., Smith, J.V., 1968. Crystal structures of natural olivines. *Am. Mineral.* **53**, 807–824.

Carroll, M.R., Webster, J.D., 1994. Solubilities of sulfur, noble gases, nitrogen, chlorine and fluorine in magmas. In: Carroll, M.R., Holloway, J.R. (Eds.), *Volatiles in Magmas*, vol. 30. Mineralogical Society of America.

Clayton, R.N., Mayeda, T.K., 1996. Oxygen isotope studies of achondrites. *Geochim. Cosmochim. Acta* **60**, 1999–2017.

Cotten, J., Ledez, A., Bau, M., Caroff, M., Maury, R.C., Dulski, P., Fourcade, S., Bohn, M., Brousse, R., 1995. Origin of anomalous rare-earth element and yttrium enrichments in subaerially exposed basalts—evidence from French-Polynesia. *Chem. Geol.* **119** (1–4), 115–138.

Crozaz, G., Floss, C., Wadhwa, M., 2003. Chemical alteration and REE mobilization in meteorites from hot and cold deserts. *Geochim. Cosmochim. Acta* **67** (24), 4727–4741.

Evensen, N.M., Hamilton, P.J., Onions, R.K., 1978. Rare-earth abundances in chondritic meteorites. *Geochim. Cosmochim. Acta* **42** (8), 1199–1212.

Floran, R.J., Prinz, M., Hlava, P.F., Keil, K., Nehru, C.E., Hinthorne, J.R., 1978. Chassigny meteorite—cumulate dunite with hydrous amphibole-bearing melt inclusions. *Geochim. Cosmochim. Acta* **42** (8), 1213–1229.

Franchi, I.A., Wright, I.P., Sexton, A.S., Pillinger, C.T., 1999. The oxygen isotopic composition of Earth and Mars. *Meteorit. Planet. Sci.* **34**, 657–661.

Goodrich, C.A., Herd, C.D.K., Taylor, L.A., 2003. Spinels and oxygen fugacity in olivine-phyric and lherzolitic shergottites. *Meteorit. Planet. Sci.* **38**, 1773–1792.

Hawthorne, F.C., 1981. Crystal chemistry of amphiboles. In: Veblen, D.R. (Ed.), *Reviews in Mineralogy*, vol. 9A. Mineralogical Society of America, Washington.

Herd, C.D.K., Borg, L.E., Jones, J.H., Papike, J.J., 2002. Oxygen fugacity and geochemical variations in the Martian basalts: implications for Martian basalt petrogenesis and the oxidation state of the upper mantle of Mars. *Geochim. Cosmochim. Acta* **66** (11), 2025–2036.

Herd, C.D.K., Treiman, A.H., McKay, G.A., Shearer, C.K., 2005. Light lithophile elements in Martian basalts: evaluating the evidence for magmatic water degassing. *Geochim. Cosmochim. Acta* **69**, 2431–2440.

Huang, E., Chen, C.H., Huang, T., Lin, E.H., Xu, J.A., 2000. Raman spectroscopic characteristics of Mg–Fe–Ca pyroxenes. *Am. Mineral.* **85** (3–4), 473–479.

James, O.B., Floss, C., McGee, J.J., 2002. Rare earth element variations resulting from inversion of pigeonite and subsolidus reequilibration in lunar ferroan anorthosites. *Geochim. Cosmochim. Acta* **66** (7), 1269–1284.

Johnson, M.C., Rutherford, M.J., Hess, P.C., 1991. Chassigny petrogenesis—Melt compositions, intensive parameters, and water contents of Martian magmas. *Geochim. Cosmochim. Acta* **55**, 349–366.

Jones, J.H., 2004. The edge of wetness: the case for dry magmatism on mars. *Lunar Planet. Sci. Conf.* **35**, #1798 (Abstract).

Langenhorst, F., Greshake, A., 1999. A transmission electron microscope study of Chassigny: evidence for strong shock metamorphism. *Meteorit. Planet. Sci.* **34** (1), 43–48.

Lindsley, D.H., 1983. Pyroxene thermometry. *Am. Mineral.* **68**, 477–493.

Lundberg, L.L., Crozaz, G., McKay, G., Zinner, E., 1988. Rare-Earth elements carriers in the Shergotty meteorite and implications for its chronology. *Geochim. Cosmochim. Acta* **52** (8), 2147–2163.

Malavergne, V., Guyot, F., Benzerara, K., Martinez, I., 2001. Description of new shock-induced phases in the Shergotty, Zagami, Nakhla and Chassigny meteorites. *Meteorit. Planet. Sci.* **36** (10), 1297–1305.

Mason, B., Nelen, J.A., Muir, P., Taylor, S.R., 1975. The composition of the Chassigny meteorite. *Meteoritics* **11** (1), 21–27.

McKay, G., Wagstaff, J., Yang, S.R., 1986. Clinopyroxene Ree distribution coefficients for Shergottites—the Ree content of the Shergotty melt. *Geochim. Cosmochim. Acta* **50** (6), 927–937.

McMillan, P., Akaogi, M., 1987. Raman-Spectra Of Beta-Mg_2SiO_4 (modified spinel) and Gamma-Mg_2SiO_4 (spinel). *Am. Mineral.* **72** (3–4), 361–364.

McSween, H.Y., Grove, T.L., Lentz, R.C.F., Dann, J.C., Holzheid, A.H., Riciputi, L.R., Ryan, J.G., 2001. Geochemical evidence for magmatic water within Mars from pyroxenes in the Shergotty meteorite. *Nature* **409** (6819), 487–490.

Mikouchi, T., Monkawa, A., Koizumi, E., Chokai, J., Miyamoto, M., 2005. MIL03346 Nakhlite and NWA2737 "Diderot" Chassignite: two new martian cumulate rocks from hot and cold deserts. *Lunar Planet. Sci. Conf.* **36**, #1944 (Abstract).

Miller, M.F., Franchi, A., Sexton, A.S., Pillinger, C.T., 1999. High precision $\delta^{17}O$ measurements of oxygen from silicates and other oxides: method and applications. *Rapid Commun. Mass Spectrom.* **13**, 1211–1217.

Misawa, K., Shih, C.-Y., Reese, Y., Nyquist, L.E., Barrat, J.A., 2005. Rb/Sr and Sm/Nd isotopic systematics of NWA 2737 chassignite. *Meteorit. Planet. Sci.* (Abstract).

Monkawa, A., Mikouchi, T., Koizumi, E., Chokai, J., Miyamoto, M., 2004. Fast cooling history of the chassigny martian meteorite. *Lunar Planet. Sci. Conf.* **35**, #1535 (Abstract).

Nakamura, N., Komi, H., Nishiykawa, Y., Pellas, P., 1982a. REE abundances in the Chassigny meteorite. *NIPR Sym. Antarctic Meteorites.* **7th**, 47–48.

Nakamura, N., Unruh, D.M., Tastumoto, M., Hutchison, R., 1982b. Origin and evolution of the Nakhla meteorite inferred from the Sm-Nd and U-Pb systematics and REE, Ba, Sr, Rb abundances. *Geochim. Cosmochim. Acta* **46**, 1555–1573.

Nyquist, L.E., Bogard, D.D., Shih, C.Y., Greshake, A., Stoffler, D., Eugster, O., 2001. Ages and geologic histories of Martian meteorites. *Space Sci. Rev.* **96** (1–4), 105–164.

Papike, J.J., Karner, J.M., Shearer, C.K., 2004. Comparative planetary mineralogy: $V/(Cr + Al)$ systematics in chromite as an indicator of relative oxygen fugacity. *Am. Mineral.* **89** (10), 1557–1560.

Putnis, A., 1979. Electron petrography of high-temperature oxydation in olivine from the Rhum layered intrusion. *Mineral. Mag.* **43** (326), 293–296.

Sautter, V., Barrat, J.A., Jambon, A., Lorand, J.P., Gillet, P., Javoy, M., Joron, J.L., Lesourd, M., 2002. A new Martian meteorite from Morocco: the nakhlite North West Africa 817. *Earth Planet. Sci. Lett.* **195** (3–4), 223–238.

Sun, S.S., McDonough, W.F., 1989. Chemical and isotopic systematics of oceanic basalts: implications for mantle composition and processes. In: Saunders, A.D., Norry, M.J. (Eds.), *Magmatism in the Oceanic Basin*. Geological Society special publications, London.

Treiman, A.H., 1985. Amphibole and hercynite spinel in Shergotty and Zagami Magmatic water, depth of crystallization, and metasomatism. *Meteoritics* **20**, 229–243.

Treiman, A.H., Gleason, J.D., Bogard, D.D., 2000. The SNC meteorites are from Mars. *Planet. Space Sci.* **48**, 1213–1230.

Wadhwa, M., 2001. Redox state of Mars' upper mantle and crust from Eu anomalies in shergottite pyroxenes. *Science* **291** (5508), 1527–1530.

Wadhwa, M., Crozaz, G., 1995. Trace and minor elements in minerals of Nakhlites and Chassigny—clues to their petrogenesis. *Geochim. Cosmochim. Acta* **59** (17), 3629–3645.

Watson, L.L., Hutcheon, I.D., Epstein, S., Stolper, E.M., 1994. Water on mars—clues from Deuterium/Hydrogen and water contents of hydrous phases in SNC meteorites. *Science* **265**, 86.

Wentworth, S.J., Gooding, J.L., 1994. Carbonates and sulfates in the Chassigny meteorite: further evidence for aqueous chemistry on the SNC parent planet. *Meteoritics* **29**, 860–863.

Zinner, E., Crozaz, G., 1986. A method for the quantitative measurement of rare-earth elements in the ion microprobe. *Int. J. Mass Spectrom. Ion Proc.* **69** (1), 17–38.